Combustion and Flame 274 (2025) 113948

Contents lists available at ScienceDirect

Combustion and Flame

journal homepage: www.sciencedirect.com/journal/combustion-and-flame

Hypergolic ignition of hybrid rocket fuels in a slab burner experiment

Olivier Jobin *, Mathieu Chartray-Pronovost, William Kaprolat, Étienne Robert

Polytechnique Montréal, 2900 Boulevard Édouard-Montpetit, Montréal, QC H3T 1J4, Canada

ARTICLE INFO

Keywords:
Hypergolic ignition
Hybrid rocket
Slab burner
Paraffin
Ammonia borane

ABSTRACT

Hypergolic ignition systems, where combustion is initiated nearly instantaneously upon contact between the oxidizer and the fuel, can improve the reliability, safety, and simplicity of hybrid rocket engines. Hypergolic performance, first and foremost the ignition delay, is of critical importance as it determines the response time of the propulsion system. To evaluate this performance metric, a novel slab burner experiment is developed to study the hypergolic behavior of hybrid rocket propellants in an engine-like configuration. The liquid oxidizer injection system and the flow conditions implemented in this slab burner are characterized in detail. Two types of experiments are presented. In the first, nitric acid is used essentially for ignition and is injected as a spray into a combustion chamber containing a paraffin-based fuel slab doped with ammonia borane and filled with gaseous oxygen. Rapid hypergolic ignition, in the order of 250 to 3000 ms, with nitric acid and sustained combustion with gaseous oxygen are observed. In the second experiment, concentrated nitric acid is injected into a combustion chamber under an inert atmosphere resulting in significantly slower ignition. The experiments are filmed with a high-speed camera to measure the hypergolic ignition delays and the location of flames. Additionally, the reignition capability of these two systems is evaluated. Successful reignitions are observed with delays greater than the initial hypergolic event.

Novelty and significance

This study presents an in-depth investigation of hypergolic ignition in hybrid rocket engines. A novel hypergolic slab burner experiment is designed and presented. This experimental setup allows for a detailed analysis of hypergolic ignition delays and combustion dynamics in hybrid rocket propellants, providing valuable insights for improving hypergolic engine reliability and performance. This test configuration allows for providing insights more relevant to oxidizer injection conditions encountered in full-scale hybrid engines. In addition, hypergolic reignition performance are evaluated.

1. Introduction

Hybrid rocket engines have the potential to ease access to space through their inherent safety and simplicity of operation compared to solid or liquid rocket engines. One way to further enhance the simplicity and reliability of hybrid propulsion is through the use of hypergolic ignition systems. These allow the elimination of complex and heavy ignition mechanisms such as spark igniters or pyrotechnics. In addition, a hypergolic ignition system gives the engine re-ignition capability, which is desirable for various missions and operations, such as in-space propulsion for intermediary burns, orbital correction maneuvers, and reaction control systems (RCS).

The introduction of hypergolicity into hybrid rocket engines is typically accomplished by embedding additives in a fuel binder. These additives exhibit hypergolic behavior with the oxidizer, ideally achieving ignition within milliseconds of initial contact between the reactants. Notable hypergolic additives include ammonia borane (AB, BH_3NH_3) [1–7], metal–organic frameworks [8–10], sodium amide ($NaNH_2$) [11], sodium borohydride ($NaBH_4$) [12–14] and potassium bis(trimethylsilyl) amide (PBTSA, $KSI_2C_6NH_{18}$) [11]. For hybrid propulsion systems, they are usually incorporated into a fuel such as paraffin wax, low or high-density polyethylene (LDPE or HDPE, respectively), or sorbitol. Investigated oxidizers are mainly some type of nitric acid (HNO_3) such as concentrated nitric acid, white fuming nitric acid (WFNA) or red fuming nitric acid (RFNA), concentrated hydrogen peroxide (H_2O_2), nitrogen tetroxide (NTO, N_2O_4) or mixed oxides of nitrogen (MON).

Droplet ignition tests are a simple and convenient experiments for evaluating the hypergolic behavior of fuel-oxidizer combinations. In this test configuration, a large oxidizer droplet is generated from a syringe and is released from a fixed height, ultimately impacting a fuel

* Corresponding author.
E-mail addresses: olivier.jobin@polymtl.ca (O. Jobin), mathieu.chartray-pronovost@polymtl.ca (M. Chartray-Pronovost), william.kaprolat@polymtl.ca (W. Kaprolat), etienne.robert@polymtl.ca (É. Robert).

https://doi.org/10.1016/j.combustflame.2024.113948
Received 7 September 2024; Received in revised form 20 December 2024; Accepted 24 December 2024
Available online 15 January 2025

pellet containing the hypergolic additives. The ignition is then recorded with a high-speed camera or other detector to measure time delay between the initial contact of the two propellants and the emergence of the first visible flame. In this configuration, interesting parameters such as droplet velocity, diameter, fuel surface roughness, storage conditions, additive content in the fuel, additive granulometry and ambient pressure have been identified as influencing the ignition delay [4, 14,15]. Although useful for evaluating the ignition delay, this type of experiment does not reflect the conditions encountered in hybrid engines, namely oxidizer injection as a gas or through multiple small droplets, shear flow at the fuel surface, turbulence, and the enclosed volume. In fact, such droplet ignition experiments are often conducted under ambient atmosphere with air as the surrounding gas. As highlighted by Nath et al. [14], the medium in which the experiments are conducted greatly affects the ignition delay of hypergolic fuels. For droplet ignition test using H_2O_2 and $NaBH_4$, they measured an ignition delay 48% lower when argon was used as the surrounding gas, as opposed to air, and that helium completely inhibited the ignition, likely as a result of its high thermal diffusivity.

Recent studies have begun to evaluate hypergolic performance under engine-like conditions. A previous study by Jobin et al. [6] and the work of Nath et al. [16] investigated the hypergolic ignition of hybrid fuels under oxidizer sprayed from injectors, as can be the case in an engine. Both groups reported higher ignition delays compared to droplet ignition tests. Nath et al. used an additive content of 25 wt% $NABH_4$ in a HDPE fuel matrix and 90% hydrogen peroxide injected at a rate of 2.5 ml/s. They performed a single ignition test in which they observed multiple ignition kernels lasting 3 to 5 ms, but no sustained flame. In our previous experiments using AB and paraffin fuel samples and concentrated nitric acid as the oxidizer, the results showed a relationship between the ignition delay and the droplet Weber number of the sprayed oxidizer [6]. In this case, a Phase Doppler Anemometer (PDA) system was used to measure the conditions across the spray from three different injection nozzles. An increase in velocity tended to decrease the ignition delay, likely due to the droplets covering more of the surface with a thinner layer of liquid as they hit the sample. In these experiments, ignition delays ranging from 24 to 1138 ms were measured depending on the spray conditions, with most of the sample undergoing sustained combustion.

Two recent investigations have tested a hypergolic ignition system in an engine-like configuration. Benhidjed-Carayon et al. [17] designed and tested a 2-in diameter engine to evaluate the combustion and ignition performance of a paraffin-based fuel with either sodium amide or PBTSA as the hypergolic additive and MON-3 as the oxidizer. They reported stable combustion, high performance and low ignition delays on the order of 100 to 200 ms. The additive content varied throughout the length of the fuel, with the first section where the oxidizer directly impinges on the fuel having a 90 wt% hypergolic additive content. In addition, they were able to successfully demonstrate the reignitability of the engine. However, having such a high additive content resulted in a locally excessively high regression rate. They concluded that in this configuration, a combustion time greater than 2 s would not be sustainable due to increased instabilities, necessitating the need for other additives with lower regression rates or an improved ignition segment geometry and design.

Jeong et al. [18] designed a 25 wt.%AB, 1 wt% palladium-carbon (Pd-C) and 74 wt% paraffin igniter for a laboratory-scale hybrid rocket engine using 95 wt% H_2O_2 as the oxidizer. The igniter was placed in the upstream section of an optically accessible poly(methyl methacrylate) (PMMA) engine. The Pd-C additive helps to reduce the ignition delay due to the catalytic properties of Pd with hydrogen peroxide. Thus, this igniter relies on both the hypergolic reaction between AB and H_2O_2 as well as the catalyzed thermal decomposition of H_2O_2 when in contact with the palladium.

The use of laboratory-scale engines, as in these two studies, is a valuable method for evaluating rocket performance parameters such as specific impulse (I_{sp}) or characteristic velocity. However, in the first investigation, the lack of optical access prevents the visualization and analysis of the hypergolic ignition in an engine configuration. In the study performed by Jeong et al. [18], although their engines were optically accessible due to the translucency of PMMA, the igniters burned out completely after only a few seconds, making engine relighting impossible. These observations therefore justify the need to perform visually accessible hypergolic tests in an engine-like configuration, which is the focus of this paper.

The first objective of this study is to design a novel hypergolic slab burner that allows the visualization of the ignition process in a configuration close to those encountered in a hybrid engine. It implements an injection system that accommodates a liquid oxidizer. In this case, the oxidizer used is 90 wt% concentrated nitric acid, whereas the fuel is paraffin wax with ammonia borane (AB) as the hypergolic additive. The spray ignition is characterized in detail using a PDA system. The hypergolic slab burner can be operated in two modes, representing different scenarios. The first is the use of nitric acid for ignition, in conjunction with a secondary oxidizer, gaseous oxygen (GOx) in this case, to sustain combustion of the paraffin-based fuel. The second mode of operation is to provide only the liquid oxidizer in the combustion chamber, both to initiate the combustion and to sustain it. The novel research facility is then used to observe and characterize the hypergolic ignition process, quantifying critical parameters such as the ignition delay and its location along the fuel slab. The location is compared against the results from the spray injector characterization campaign. The flame intensity and its location over the fuel length is also discussed. The reignition of the fuel slabs is investigated and successfully demonstrated. Finally, the regression rate of the fuels compositions is presented.

2. Materials and methods

2.1. Slab burner visualization experiment

The slab burner used for this work is adapted from previous experiments conducted at Polytechnique Montréal [19]. The test facility consists of three sections: a stabilization chamber and a combustion chamber, with a new spray injection section introduced between them. A picture and a schematic representation of the slab burner are shown in Figs. 1 and 2. The design of the stabilization and the combustion chambers are already discussed in a previous research article [19], but the injection section is discussed in further details here since it is part of the novelty of this work.

The injection plate is a square measuring 254 mm by 254 mm and is 31.8 mm thick. It has an opening in the center with the same dimensions as the combustion chamber, i.e., a square cross-section of 50.8 by 50.8 mm. The part is made of the same material as the other parts of the slab burner, 304L stainless steel. On the top of the square channel, a 101.6 mm (4 in.) long hole extends from the opening to the top of the plate. A 1/4 in. diameter stainless steel tube (Swagelok, USA) is inserted into this hole. The tube is secured to the top with an NPT fitting, and its other end is bent at a 90-degree angle to enter the combustion chamber. An injector (MC41024, Mistcooling, USA) is secured onto the end of the tube. It has a diameter of 0.3 mm and the flow pattern results in a full cone spray. This injector was selected for its small outside diameter, low flow rate, and compatibility with concentrated nitric acid.

Since the injector is placed directly in the flow coming out of the stabilization chamber, its diameter footprint had to be as small as possible to avoid large turbulent flow structures induced by its presence. Section 3.2 covers the characterization of the flow field in the presence of the injection system. Finally, the injection tube is connected to a pressurized nitric acid tank as shown in the Piping and Instrumentation Diagram (P&ID) of Fig. 3. The mass flow rate of nitric acid is controlled by changing its static pressure in the tank.

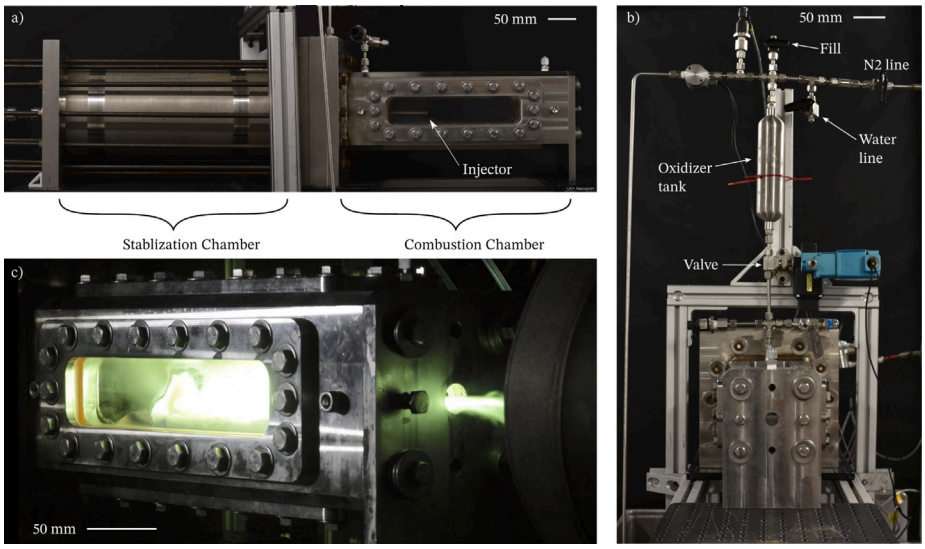

Fig. 1. (a) Side view of the hypergolic slab burner. (b) Front view of the burner. (c) A test in the hypergolic slab burner.

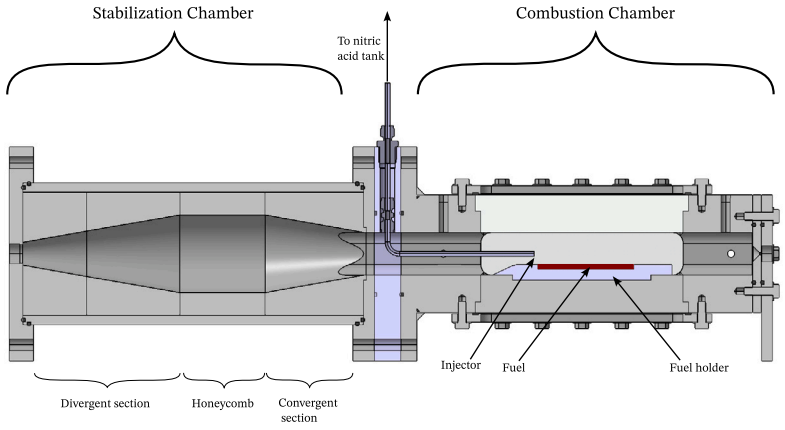

Fig. 2. Detailed section view of the hypergolic slab burner.

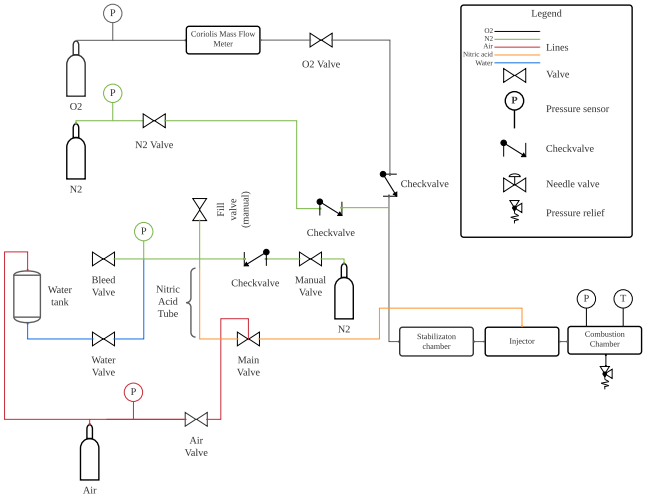

Fig. 3. Piping & instrumentation diagram of the hypergolic slab burner.

2.2. Fuel preparation

The fuel is composed of paraffin wax (FR5560, Candlewic, USA) and ammonia borane (#900–1016, Boron Specialties LLC, USA). The paraffin is received in slabs while AB is purchased in powder form. The paraffin is ground into powder using an electric blade grinder, into which a small amount of dry ice is added with the paraffin. The dry ice prevents powdered paraffin from reagglomerating due to the heat generated by the friction of the blades. Both powders are then sieved through meshes to obtain a granulometry of 212–500 μm. The components are weighed using a milligram scale (NewClassic MF MS304S/03, Mettler Toledo, Switzerland) and thoroughly mixed in a custom Y-mixer to the desired mass ratio. Approximately 25 g of the fuel mixture is placed in a rectangular press mold measuring 114.3 mm (4.5 inches) by 50.8 mm (2.0 inches) with a thickness of 12.7 mm (0.5 inches). The mold is placed and pressed in a 20-ton hydraulic press (Model M, Carver Laboratory Press, USA). Both the fuel slabs and the pure ammonia borane are stored in a closed container with desiccant to ensure that the samples do not adsorb moisture that could affect their ignition performance. The samples are only exposed to ambient air when they are transferred from the closed containers to the combustion chamber, minimizing the time they could be exposed to humidity. Prior to insertion into the slab burner, the fuel slab surface is lightly brushed to remove any remaining powder or impurities on the surface. The surface is left intact, neither cut nor sanded. The fuel slab

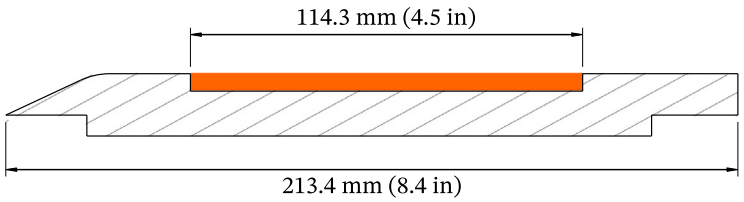

Fig. 4. Side view of the fuel holder with the fuel represented as the orange rectangle. The width of the assembly is 50.8 mm (2 in), the same as the combustion chamber.

is glued to a 304L stainless steel fuel holder. The fuel slab is fixed to the fuel holder in such a way that its surface is not protruding from the holder. The fuel holder has a shape similar to what is commonly reported in the literature with a forward facing ramp of 25 degrees, which reduces instabilities and recirculation zones as opposed to a sharp leading edge [20,21]. The fuel holder design is shown in Fig. 4.

2.3. Video acquisition and analysis

The experiments are filmed with a high-speed camera (Fastcam Mini AX200, Photron, Japan) at a rate of 1000 frames per second. The camera is pointed toward the inside of the combustion chamber, covering the entire fuel slab. A 105 mm lens is mounted on the camera, which typically results in a spatial resolution of approximately 10 pixels per mm. The high-speed camera video is analyzed to determine the ignition delay, defined as the time between the first droplets exiting the nozzle and the first flame, with a typical first contact time of approximately 3 to 5 ms. The location of the first ignition kernel is also identified to correlate ignition with oxidizer spray dynamics.

2.4. Tests procedure

First, the hypergolic slab burner is used to evaluate the suitability of a hypergolic igniter system in a paraffin/oxygen hybrid engine. In this case, an oxygen flow is stabilized in the test section by supplying oxygen for a few seconds before a small amount of nitric acid, 5 to 10 ml, is sprayed through the injector. The hypergolic reaction between AB and the nitric acid is sufficient to melt the paraffin and initiate the slab combustion. After a set time, usually 3 s, the nitric acid spray is stopped and the fuel reacts only with gaseous oxygen.

In the second test configuration, the combustion chamber is filled with nitrogen prior to nitric acid injection to ensure that ambient air does not contribute to the ignition or to the sustained combustion. The pressurized nitric acid is then sprayed into the chamber, initiating hypergolic ignition. Combustion is maintained as long as the nitric acid continues to be sprayed. The test is terminated after 10 s when the injection of oxidizer is stopped.

In both cases, the flame is quenched by purging the stabilization and combustion chambers with nitrogen at the end of the test. Before removing the fuel sample, the nitric acid tank and injector are rinsed with distilled water. Extensive safety precautions are taken during the tests, including the wearing of acid-resistant gloves, boots, and a protective hazmat suit (Tychem 5000, DuPont, USA) sealed with nitric acid-resistant tape, and a face shield with organic vapor cartridges.

In both test configurations, the reignition is evaluated by performing the test procedure a second time without removing the fuel slab from the chamber. However, as a safety measure, only the amount of nitric acid required for one test is loaded and pressurized into the oxidizer tank. The oxidizer tank is refilled and pressurized between the initial ignition and reignition tests, a process that takes approximately 30 min. This also ensures that the combustion chamber and fuel slab temperatures return to ambient conditions prior to reignition attempts.

A summary of the test sequences and test parameters are presented in Fig. 5 and Table 1 respectively. Similarly, the reignition experiments utilize the identical test sequence employed in the initial ignition test. The results of the first experiment are presented in Section 3.3 whereas the results for the second experiment are presented in Section 3.4. The reignition results are discussed in Section 3.5.

3. Results

3.1. Spray characterization

The oxidizer injector mass flow is first characterized at three different tank pressures (0.68 MPa, 1.72 MPa and 3.45 MPa) using water as a surrogate for nitric acid due to its highly corrosive nature. This method allows the mass flow to be estimated using only the gas pressure, without the use of a flow meter. First, the water is pressurized with nitrogen to a given pressure. A valve located between the injector and the water tank is then opened. The mass flow is measured using a Coriolis mass flow meter (mini CORI-FLOW^{TM} M15, Bronkhorst, The Netherlands). The valve is left opened for a few seconds to allow the mass flow signal to stabilize and the procedure is repeated for all pressures with the results are shown in Fig. 6(a). A fitted curve in the form of $y = mx^n$ is calculated with an R^2 value of 0.981 and an exponent n equal to 0.49. Finally, the results are converted from a water mass flow rate to a nitric acid flow rate using the following equation:

$$\dot{m} = C_d A \sqrt{2\rho \Delta P} \tag{1}$$

where $\dot{m}$ is the mass flow, C_d is the discharge coefficient, A is the injector area, ρ is the density of the fluid, and ΔP is the static pressure difference between ambient conditions and the water tank pressure. When water is used as the fluid, C_d is calculated knowing all the other parameters. For the tested injector, C_d is 0.318 ± 0.012 and is constant over the tested pressure range. For a pressure swirl injector, C_d is independent of the Reynolds number (Re) for values above 3000, which is the case for the test conditions here [22]. Thus, using this discharge coefficient value, the steady-state water mass flow is converted in a steady-state nitric acid mass flow by knowing its density and pressure during the slab burner tests. This allows the mass flow to be obtained even though the acid is not compatible with the Coriolis flow meter. The Re and Weber (We) numbers are also calculated as they are important non-dimensional parameters related to spray atomization, calculated using the following equations:

$$Re = \frac{\rho U d_{inj}}{\mu} \tag{2}$$

$$We = \frac{\rho U^2 d_{inj}}{\sigma} \tag{3}$$

with $U = 4\dot{V}/\pi d_{inj}^2$ and $\dot{V} = \dot{m}/\rho$, U is the velocity of the spray exiting the injector, d_{inj} is the diameter of the injector, μ is the dynamic viscosity, σ is the surface tension between the liquid and the surrounding media, and $\dot{V}$ is the volumetric flow rate.

A PDA system (112 mm Fiber PDA and FlowExplorer laser, Dantec Dynamics, Denmark) is also used to characterize the spray parameters. Measurements are taken with water and with the injector inside the combustion chamber of the slab burner, with and without the use of an oxidizer co-flow. They are conducted at the center of the spray coming out of the injector at a fixed height, corresponding to the fuel height, i.e., the location where the oxidizer droplets hit the fuel surface and subsequently lead to hypergolic ignition. The rationale of these measurements is to determine the droplet conditions that lead to ignition. The PDA is mounted on a traverse system (Lightweight Traverse, ISEL, Germany) to allow scanning in the longitudinal directions. The scans are performed at each point in space for 180 s

Table 1
Summary of test conditions for both configurations.

	Experimental configuration 1	Experimental configuration 2
Oxidizer	GOx/Nitric acid	Nitric acid
Purge	GOx, 5s before nitric acid injection	N_2, 5s before nitric acid injection
AB% content	20 and 40	40
Reignition	Yes	Yes

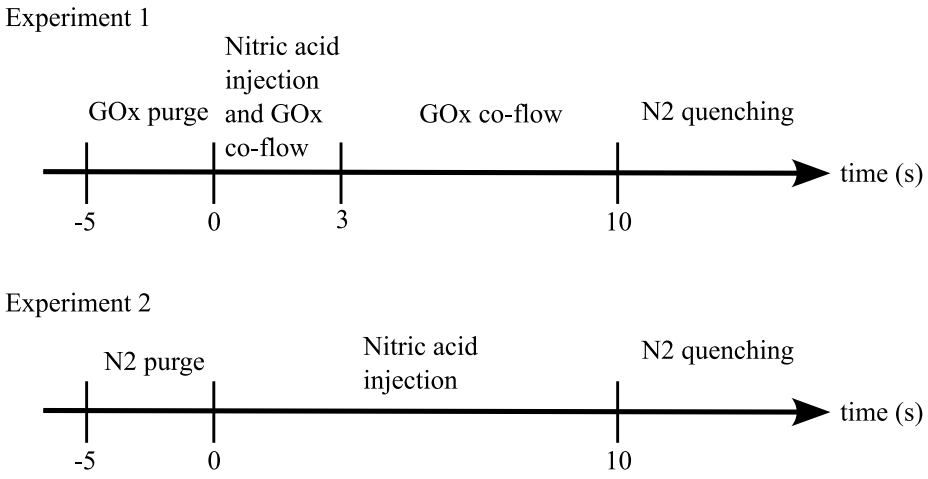

Fig. 5. Test sequence for both experiment conducted.

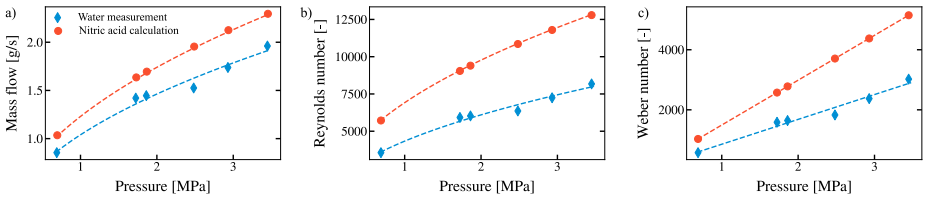

Fig. 6. Experimental results using the mass flow meter. (a) The mass flow as a function of the tank static pressure. (b) Reynolds number as a function of the tank static pressure. (c) Weber number as a function of the tank static pressure.

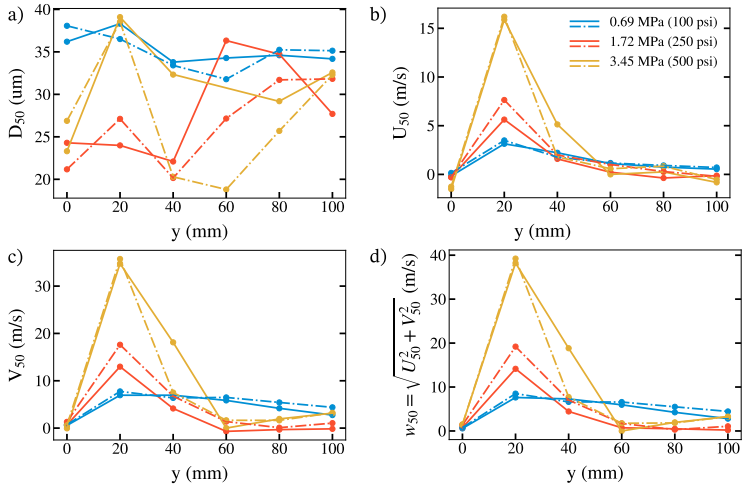

Fig. 7. Spray results from the PDA system. (a) Median diameter (b) Median horizontal velocity. (c) Median vertical velocity (d) Median total velocity. Solid line (▬▬) refers to the tests when GOx co-flow is used, dashed line (▬ ▬ ▬) refers to the conditions when only the liquid spray is present.

or for 5,000 detected droplets, whichever comes first. The PDA is operated in forward scattering mode, with an angle set to 30°, using a 300 mm lens for the laser and a 310 mm lens for the detector. Six longitudinal positions are measured for each pressure. The measured median velocities and median droplet diameters (D_{50}) are shown in Fig. 7.

Fig. 7(a) reveals that the median droplet diameter is largest at an injection pressure of 0.69 MPa (100 psi) and remains approximately constant along the length of the fuel slab. As the injection pressure is increased, a variation of D_{50} is observed along the length of the fuel, with droplets generally smaller than at 0.69 MPa (100 psi). This is due to the spray exiting the injector at a higher velocity, resulting in a

Table 2
Equivalent water pressure required to match the *Re* or *We* numbers of the nitric acid pressure.

HNO_3 Pressure [MPa (psi)]	Equivalent H_2O pressure [MPa (psi)]	
	Re similarity	We similarity
0.34 (50)	0.88 (127)	0.70 (101)
0.69 (100)	1.76 (255)	1.40 (203)
1.38 (200)	3.52 (510)	2.79 (405)
1.72 (250)	4.39 (637)	3.50 (507)

higher *We* number and increased atomization efficiency. Adding the GOx co-flow does not drastically change the D_{50} values. The median droplet diameter is approximately 37 μm for a water injection pressure of 0.69 MPa (100 psi) and between 20 and 40 for pressures varying from 1.72 MPa (250 psi) to 3.45 MPa (500 psi). Fig. 7(b) to 7(d) clearly illustrate the region where the droplets hit the fuel slab at the highest velocity, with the median total droplet velocity (w_{50}) maximum 20 mm from the injector tip, maximum values of 7.6, 14.1, and 38.2 m/s are obtained for water pressures of 0.69 MPa (100 psi), 1.72 MPa (250 psi), and 3.45 MPa (500 psi), respectively, without the GOx co-flow. The addition of the co-flow slightly increases w_{50} to maximum values of 8.5, 19.2, and 39.2 m/s.

To directly compare the results from the PDA system using water to nitric acid as the fluid, a similarity study is performed. This method relies on comparing results based on the Weber number, as opposed to the *Re* number, since the former is a more relevant similarity parameter for the atomization process [22]. The Weber number similarity comparison follows the methodology used by Indiana et al. [23] to estimate the size and velocity distributions of the nitric acid droplets in the spray.

First, the spray velocity of a nitric acid is calculated using the Bernoulli equation for a range of pressures:

$$U = (2\Delta P/\rho)^{0.5} \tag{4}$$

using the physical properties of density, dynamic viscosity, and surface tension of nitric acid. Corresponding *Re* and *We* are computed using Eqs. (2) and (3), where the previously calculated velocity is factored by the discharge coefficient of the injector. Finally, water and nitric acid static pressures which give the same *Re* and *We* are identified and are shown in Table 2. The droplet diameter and velocity in the spray is expected to follow the same behavior, i.e., the same D_{50} and w_{50}, at the same Weber number, regardless of the fluid. This methodology allows spray characterization studies to be performed in a safer manner by using water instead of nitric acid to conduct the experiments, obtaining information that is then applicable to the nitric acid tests.

3.2. Flow field characterization

The presence of the injector tube in the combustion chamber can create unwanted turbulence in the flow and act as a passive mixing device that increases the regression rate of the fuel [24] when tests are conducted using GOx. It is then not possible to use previous velocity and turbulence intensity profiles obtained using hot wire anemometry in the combustion chamber and reported in Jobin et al. [19]. Furthermore, the presence of the tube inside the chamber complicates the use of a hot wire anemometry probe to extract velocity measurements. Therefore, the velocity measurements are also performed using the PDA system with the configuration parameters presented above. First, the flow is seeded with Di-Ethyl-Hexyl-Sebacat (DEHS) aerosol droplets with a mean diameter of 0.8 μm produced by an aerosol generator (Atomizer Aerosol Generator ATM 221, Topas GmbH, Germany). The aerosol is injected before entering the stabilization chamber. These droplets are good tracers for velocity measurements since they follow the streamlines of the flow due to their small diameter.

The PDA system is used to measure the velocity of DEHS droplets passing through a measurement volume. The PDA is also mounted on

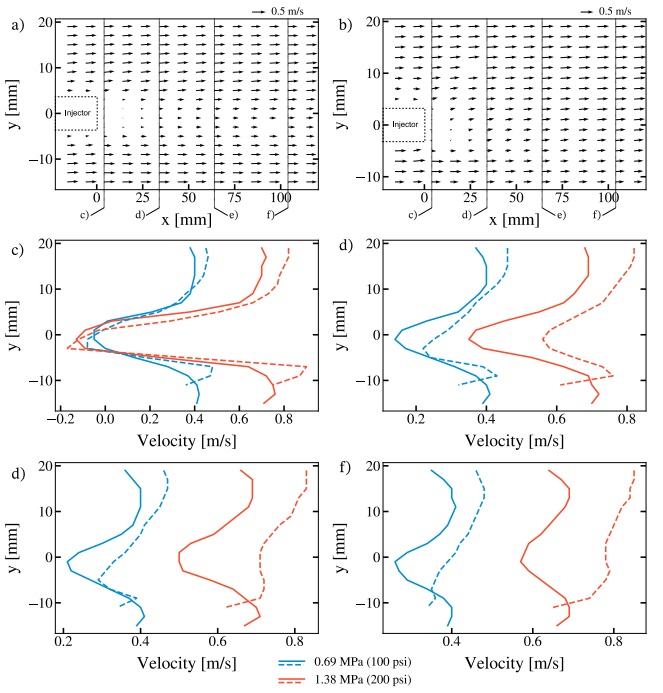

Fig. 8. Flow field and velocity slices in the combustion chamber at two GOx co-flow static pressures. x = 0 mm is positioned at the tip of the nozzle. (a) Flow field at 0.69 MPa (100 psi), without slab. (b) Flow field at 0.69 MPa (100 psi), with slab. (c) Velocity slice at x = 4 mm. (d) Velocity slice at x = 34 mm. (e) Velocity slice at x = 64 mm. (f) Velocity slice at x = 104 mm. ▬▬ refers to experiments conducted without a slab fuel, - - - - - - refers to experiments conducted with a slab fuel.

a traverse, this time to allow scanning in both the fuel longitudinal and vertical directions. The scan sheets are taken at the mid-plane of the lateral direction of the combustion chamber. In total, 252 spatial positions are scanned, with 14 positions in the longitudinal direction and 18 in the vertical direction, corresponding to spatial increments of 10 mm and 2 mm, respectively. The scans are performed at each spatial position for 60 s or for 10,000 detected droplets, whichever comes first. The turbulence in the flow is also quantified through the relative turbulence intensity, which is calculated using the following equation:

$$T = \frac{V_{rms}}{\bar{V}} \tag{5}$$

where V_{rms} is the root mean square of the velocity at a given scanning position and $\bar{V}$ is the average velocity taken at a slice of a given y position. In total, 2 velocity maps are obtained corresponding to different oxidizer velocities, which in turn are related to two static pressures and flow rate of GOx, i.e., 0.88 g/s at 0.69 MPa (100 psi) and 2.13 g/s at 1.38 MPa (200 psi). The results show that the presence of the injector affects the flow around it. The velocity downstream of the injector approaches zero immediately after it and gradually increases as shown in Fig. 8. This behavior is less pronounced when the fuel holder is placed in the combustion chamber. The flow stabilizes more quickly compared to when it is not present. In addition, the turbulence intensity is at its maximum values around the injector and decreases as the flow stabilizes. Again, the presence of the fuel geometry also tends to slightly reduce the turbulence intensity as shown in Fig. 9. The flow velocity is about 0.4 m/s at a static pressure of 0.69 MPa (100 psi) and approximately 0.7 m/s at a static pressure of 1.38 MPa (200 psi). The turbulence intensity is about 5% at a co-flow pressure of 0.69 MPa (100 psi), and between 10% to 15% at 1.38 MPa (200 psi).

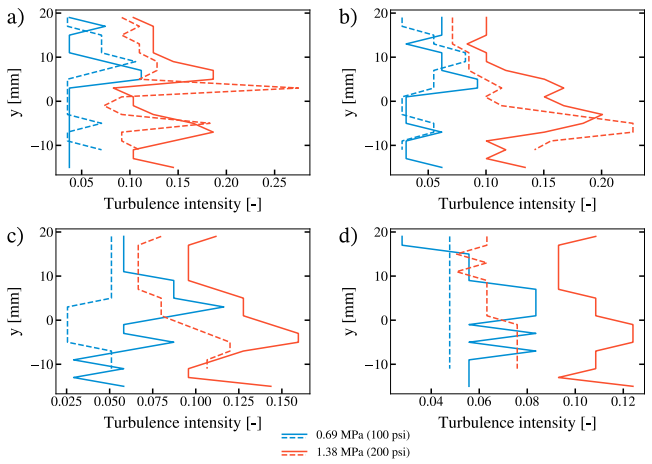

Fig. 9. Turbulence intensity slices in the combustion chamber. The pressure is the GOx co-flow pressure. x = 0 mm is positioned at the tip of the nozzle. (a) x = 4 mm. (b) x = 34 mm. (c) x = 64 mm. (d) x = 104 mm. ▬▬ refers to experiments conducted without a slab fuel, - - - - - - refers to experiments conducted with a slab fuel.

3.3. Experiment 1: Hypergolic tests using GOx and nitric acid

The objective of this first experiment is to measure the hypergolic performance of a paraffin-AB fuel, with gaseous oxygen as the oxidizer and nitric acid only initially injected as a spray in the combustion chamber to induce hypergolic ignition. This configuration is interesting because paraffin/GOx is one of the most studied hybrid propellants combinations. The idea is to provide information on a useful ignition system that could be implemented in existing engines as it requires minimal design changes. Two additive concentrations in the fuel are tested in this configuration, 20 wt% and 40 wt% and the nitric acid injection pressure is set at 1.38 MPa (200 psi), corresponding to a mass flow of 1.48 g/s.

3.3.1. Visual assessment

A visual assessment of the ignition is first performed. As soon as nitric acid is injected, droplets hit the surface and begin to agglomerate to form a larger pool of oxidizer (Fig. 10b). Surface reactions between the nitric acid and the AB in the fuel heat the small pool of oxidizer leading to bubble formation (Fig. 10c). This is likely due to dehydrogenation of the ammonia borane, as discussed in Section 4. After reaching either a critical temperature or concentration, a large ignition kernel, easily observed by its bright green flame color, appears (Fig. 10d) and propagates (Fig. 10e-f) in the chamber. The combustion is sustained throughout the test, even when the nitric acid injection is stopped (Fig. 10g).

To support the visual assessment, the intensity of the green flame is quantified using the green channel of the RGB (red, green and blue) color images. The intensity is calculated both spatially and temporally to provide time and space resolved data. Vertical flame intensity slices of 1 pixel width are extracted from the frames using the following equations:

$$I(t) = \sum_{x=0}^{x=x_{max}} \sum_{y=0}^{y=y_{max}} I(x,y) \tag{6}$$

$$\bar{I}(t) = \frac{I(t)}{max(I(t))} \tag{7}$$

where I is the green channel value of the pixel in the frame, on a scale from 0 to 255, x and y are the positions (in pixels) along the fuel length and normal to the fuel edge, respectively, t is the time, and $\bar{I}$ is the normalized intensity.

Using the light intensity as a proxy, these equations allow the evolution of the combustion to be tracked. For example, Fig. 11 shows the intensity signal over the fuel length for various tests for both additive concentrations. The intensity signal slightly increases when nitric acid is sprayed in the chamber starting at t = 0. Then, a sudden and sustained increase becomes evident, associated with the green flame following ignition. In general, the intensity decreases rapidly after ignition and stabilizes afterward. Variation in intensity are observed, likely coming from the combination of combustion instabilities, and windows being gradually blocked by fuel deposits.

The intensity signal is also observed at different locations along the length of the fuel. The intensity signals follow the same trends regardless of location, as shown in the example provided in Fig. 12. These intensity signals are taken from a test in which the AB concentration is 20 wt%. The intensity measured at x = 20.5 mm shows an initial peak due to the ignition of the fuel. Similar variations are observed at each x position, indicating even combustion of the fuel along its length.

The intensity of the flame is also evaluated spatially. The equations are similar than Eqs. (6) and (7), but the spatially-resolved values are integrated over time rather than fuel length-wise position:

$$I(x) = \sum_{t=0}^{t=t_{burn}} \sum_{y=0}^{y=y_{max}} I(t,y) \tag{8}$$

$$\bar{I}(x) = \frac{I(x)}{max(I(x))} \tag{9}$$

where the variables are similar than described above.

This light intensity signal allows the comparison of the flame intensity along the fuel length over the entire burn duration. An example of this signal is shown in Fig. 13 for tests with fuel slabs containing 40 wt% AB content. In general, the spatial intensity profiles follow similar trends. The flame intensity increases downstream of the combustion chamber, corresponding to a region of higher combustion activity. A drop in the signal is observed between x = 18 mm and 40 mm, corresponding to the location where the nitric acid spray impinges the windows. It is also at this location that the view is most obstructed by melted paraffin and solid combustion products.

The location and size of the first observable ignition kernel of each tests are also studied, as indicated by the shadow zones in Fig. 13. The start and end points of the ignition location are obtained by taking the projected area of the kernel on the fuel slab. This measure has been made for all slab burner tests in this configuration. The average length of these ignition zones are 15.1 ± 1.1 mm and 14.8 ± 9.8 mm for the 20 wt% AB and 40 wt% AB tests, respectively. The larger size uncertainty in the latter can be attributed to the higher AB content in the fuel. A larger amount of AB on the surface of the fuel may introduce more variability in the size of the initial ignition kernel. The location of the projected ignition is constrained within x = 3.5 and 11.1 mm, with average distances of 9.0 ± 2.6 mm and 7.2 ± 3.2 mm for the 20 wt% AB and 40 wt% AB tests, respectively.

Finally, since the nitric acid injection pressure for these tests is 1.38 MPa (200 psi), the Weber number similarity results in Table 2 indicate that the corresponding water pressure is 2.76 MPa (400 psi) for We = 2059. Using the results obtained from the PDA (Figs. 7a) through 7(d), the nitric acid droplets that led to the first ignition kernel have a median diameter (D_{50}) between 20 and 40 μm with a median total velocity (w_{50}) between 3 and 35 m/s. The droplet size is comparable to those reported in our previous spray ignition experiment [6]. However, the median total velocity is higher in the slab burner compared to up to 8 m/s in our previous experiment.

3.3.2. Ignition delay

Finally, the oxygen flow rate is varied using fuel containing 40 wt% additives to assess its impact on the ignition delay, with results shown in Fig. 14. At the same GOx flow rate (2.22 g/s, injection pressure = 1.38 MPa), both additive contents show a similar mean ignition delay, 278 ± 10 ms for the 20 wt% content and 286 ± 17 ms for

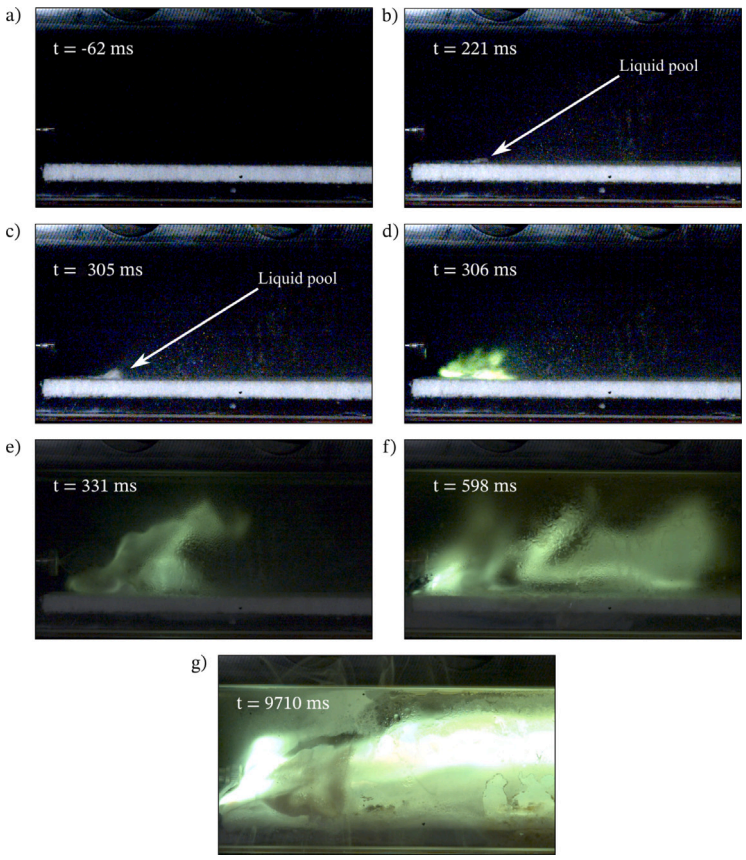

Fig. 10. Typical ignition sequence of the tests using nitric acid and GOx as the oxidizer. (For interpretation of the references to color in this figure legend, the reader is referred to the web version of this article.)

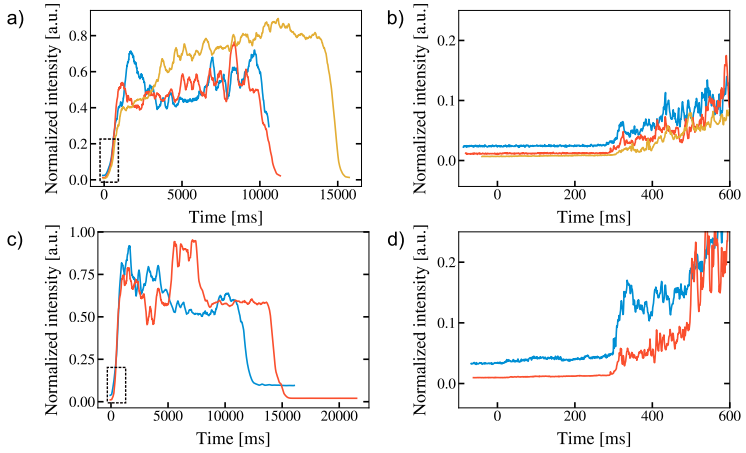

Fig. 11. Normalized flame intensity as a function of time. Each color represents a different test. (a) 40 wt% AB – 60 wt% paraffin. (b) Zoom of frame (a). (c) 20 wt% AB – 80 wt% paraffin. (d) Zoom of frame (c). (For interpretation of the references to color in this figure legend, the reader is referred to the web version of this article.)

the 40 wt% content. All samples successfully ignited and sustained combustion for the full test duration of approximately 10 s. In addition, the small standard deviation is of interest since it directly correlates with the reliability of the ignition system, which is highly desirable for hypergolic ignition. For this configuration, the ignition delay is not influenced by the additive concentration in the fuel. In fact, the limiting factor appears to be related to injection of GOx, which impacts the nitric acid droplet velocities. The effect of droplet velocity on the ignition delay was also observed in previous droplet ignition tests [4] and in oxidizer spray ignition experiments [6,16]. In the experiments presented here, as the GOx injection pressure and resulting flow rate decreases, the ignition delay and its variability generally tends to increase. It is postulated that this effect is associated with the spreading effect of the liquid oxidizer due to the co-flow. The introduction of a co-flow into the combustion chamber results in accumulated nitric acid being pushed away from the impinging location, thus increasing the fuel surface area covered by nitric acid. This has the effect of increasing the likelihood of achieving ignition conditions where a thin layer of liquid nitric acid meets a hypergolic additives in proportions appropriate to result in ignition. When the co-flow is not used, less surface area is covered by the oxidizer and achieving hypergolic ignition becomes more dependent on the impinging location conditions, such as the local AB concentration, the liquid layer thickness of nitric acid, and local heat transfer conditions.

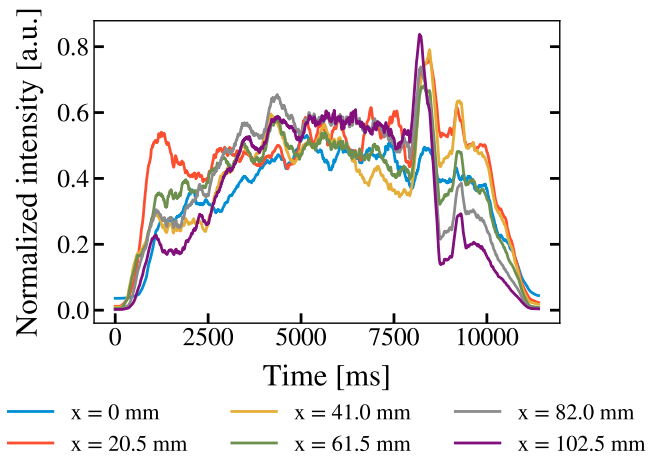

Fig. 12. Normalized flame intensity at various positions along the fuel slab length, as a function of time.

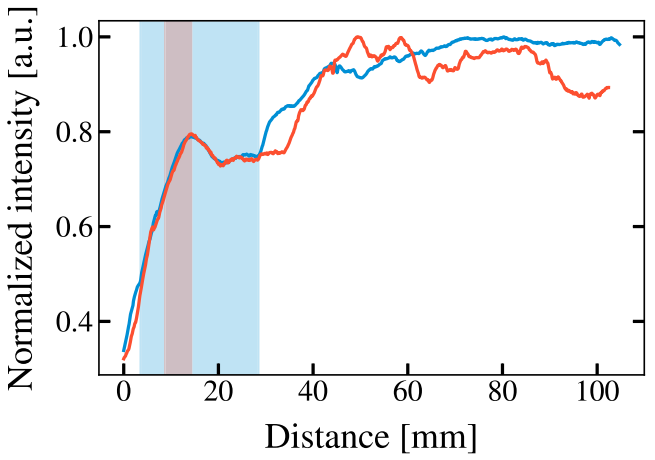

Fig. 13. Normalized flame intensity as a function of the fuel length for fuel slabs with a 40 wt% AB content. Each color represents a different test. The shadow zones are the projected area of the first ignition kernel. (For interpretation of the references to color in this figure legend, the reader is referred to the web version of this article.)

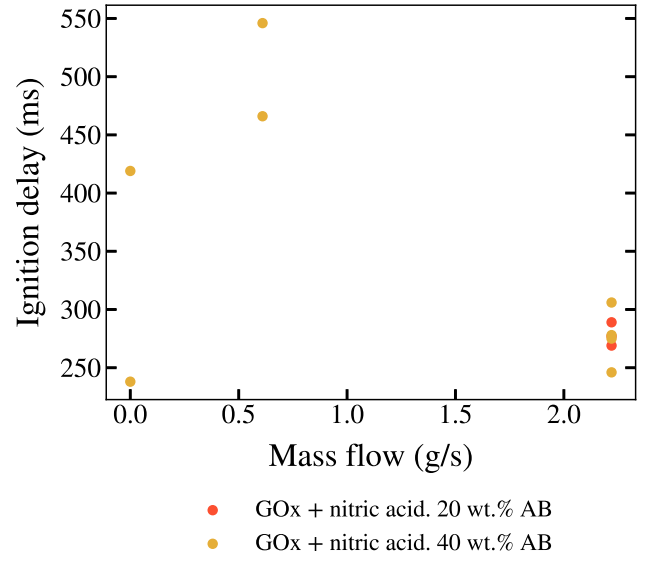

Fig. 14. Ignition delay as a function of GOx flow rate at a constant nitric acid injection mass flow of 1.48 g/s.

3.4. Experiment 2: Hypergolic tests using only nitric acid

The second set of experiments focuses on the use of nitric acid as the only oxidizer with AB-doped paraffin as the fuel. This engine configuration may be of interest for in-space propulsion, small satellites, or reaction control systems as opposed to booster engines due to the toxicity and environmental hazard of nitric acid and nitrogen oxides resulting from its decomposition and combustion. This configuration has the advantage of only having to carry nitric acid for engine operation, as opposed to carrying oxygen as well. In this case, the injection mass flow rate, is varied from 1.02 g/s (0.69 MPa, 100 psi) to 2.04 g/s (2.76 MPa, 400 psi), while keeping the AB content in the fuel slab constant at 40 wt%.

3.4.1. Visual assessment

The combustion dynamics are very different from the tests in which GOx is also used along with nitric acid. In this second test configuration, impinging nitric acid droplets also agglomerate to form a larger pool of oxidizer (Fig. 15b). Exothermic surface reactions also heat the oxidizer on the fuel surface where bubbles form (Fig. 15c). Unlike the first set of experiments however, oxidizer is scarce in the gas phase. When bubbles escape from the nitric acid, a dark orange gas fills the combustion chamber (Fig. 15d). This gas color is likely due to nitrogen dioxide (NO_2) or other N_xO_y oxides formed by the thermal decomposition of the nitric acid, in addition to water and oxygen. The hot oxygen is then available to burn with the gaseous products of the initial surface reactions, probably hydrogen as mentioned in Section 4. Ignition is however much slower than in the case where O_2 is present. After a few seconds, a small ignition kernel finally appears (Fig. 15e) and propagates, with sustained combustion (Fig. 15f) until the end of the test (Fig. 15g). As can be seen from the images in Fig. 15, the fuel surface is severely degraded as the test progresses and swelling is observed. Fig. 17(b) shows the top view of the sample burned for the test shown in Fig. 15.

To support the visual assessment, the intensity of the green channel of the RGB signal is also evaluated in this case. Due to the different combustion dynamics, a different type of intensity profile is observed as shown in Fig. 16. In this case, both the nitric acid decomposition and the ignition are captured, while previously only ignition was discussed. First, the optical signal increases for about 500 ms until it reaches a small plateau, maintained for approximately 1000 ms. Although being captured in the green channel signal, it is not related to the ignition itself, but rather to the light reflection from the oxidizer droplets. When compared to the high-speed camera images, this sequence coincides with the gradual deposition of oxidizer droplets on the windows. A sharp increase is then observed due to the production of NO_2 and N_xO_y oxides from the thermal decomposition of nitric acid. The signal decreases after approximately 1500 ms and then gradually increases and oscillates as the hypergolic ignition is triggered. The moment of ignition is using the first frame from the high-speed camera on which green ignition kernel can be seen. Interestingly, regardless of the oxidizer mass flow, the onset of nitric acid thermal decomposition and its duration are very similar, even though the ignition delays are not the same, as shown in the next section. This suggests that the limiting factor preventing rapid ignition occurs after the thermal decomposition of the nitric acid. As observed earlier, the intensity signals over the length of the fuel also follow the same trend.

Unlike the tests conducted with GOx and nitric acid as the oxidizers, the location and size of the first ignition kernel cannot be measured due to the accumulation of residues on the slab burner windows. These residues are likely a results of the nitric acid vapors as they tend to leave an opaque white film on materials. Due to the longer ignition delay compared to the first set of experiments and the lack of GOx flow, the ignition process is not well captured by the high-speed camera. However, the fuel samples at the end of the tests clearly show an area where most of the fuel was consumed. This is also the region where the

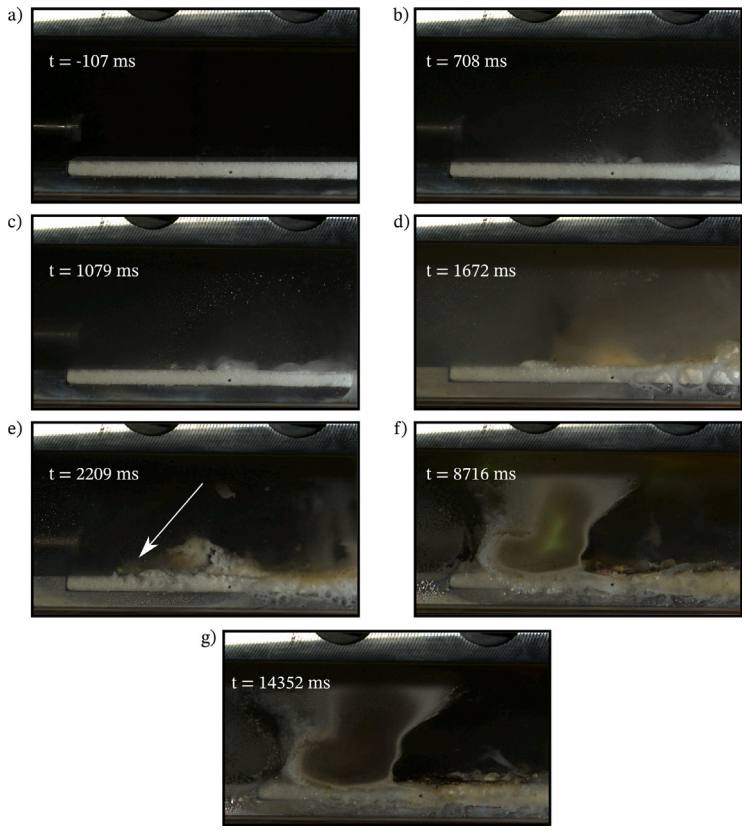

Fig. 15. Typical ignition sequence of the hypergolic slab tests using only nitric acid as the oxidizer. (For interpretation of the references to color in this figure legend, the reader is referred to the web version of this article.)

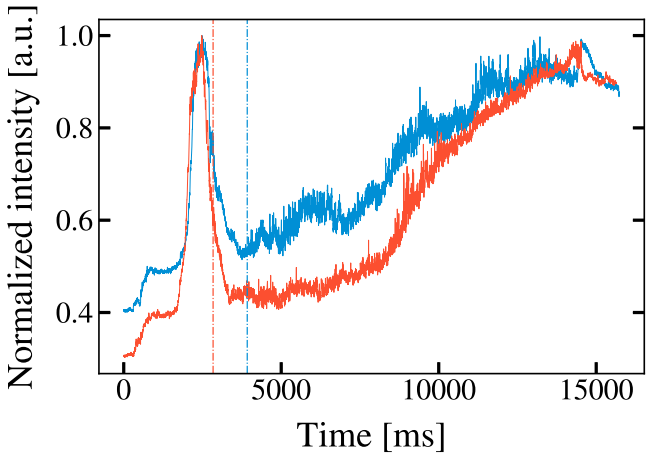

Fig. 16. Normalized flame intensity as a function of time. Each color represents a different test. The dashed lines represent the moment of ignition as defined by the appearance of a green flame. (For interpretation of the references to color in this figure legend, the reader is referred to the web version of this article.)

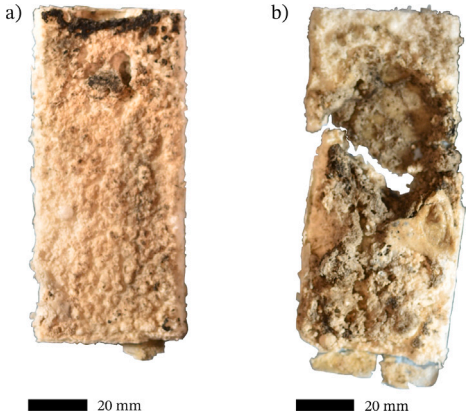

Fig. 17. Top view of examples of the fuel slab after a hypergolic test. Flow is from top to bottom. (a) A hypergolic test using nitric acid and GOx. (b) A hypergolic test using only nitric acid.

first hypergolic ignition kernels are observed. An example of the fuel after a burn is shown in Fig. 17. For the majority of tests, the fuel in this region was completely burned. However, it should be noted that after a test, for safety reasons, water is injected through the nozzle into the slab burner combustion chamber to dilute any remaining unreacted nitric acid. AB is known to be soluble in water, so the condition of the fuel slab after the test may also be affected by the water, not just the by the reaction with nitric acid.

This observation is further supported by comparing the intensity signal along the fuel length. As opposed to the first test configuration, the maximum value is located at the same position as the observed burn-through of the samples, rather than further downstream on the fuel slab. As can be seen in Fig. 18(a to c), the intensity profiles generally follow a very similar trend, showing great repeatability between tests.

3.4.2. Ignition delay

The ignition delay results are shown in Fig. 19 and are compared to the values measured when GOx was also used. Two tests are performed for each injection pressure. In all the test presented here, the ignition delay using only nitric acid is an order of magnitude higher than when GOx is also injected in the slab burner. The first three flow rates show a fairly constant ignition delay at 2987, 3379 and 2875 ms

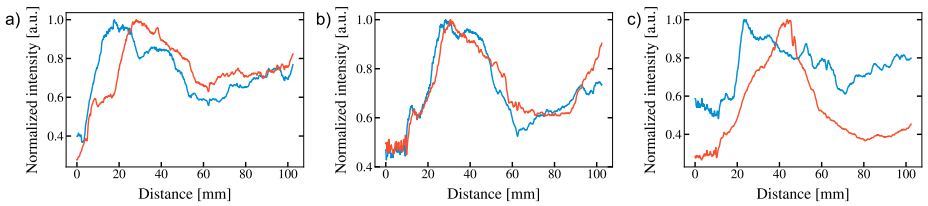

Fig. 18. Normalized intensity as a function of position along the fuel slab. Each color represents a different test. Nitric acid flow rate = (a) 1.02 g/s (0.69 MPa,100 psi). (b) 1.48 g/s (1.38 MPa, 200 psi). (c) 2.04 g/s (2.76 MPa, 400 psi). (For interpretation of the references to color in this figure legend, the reader is referred to the web version of this article.)

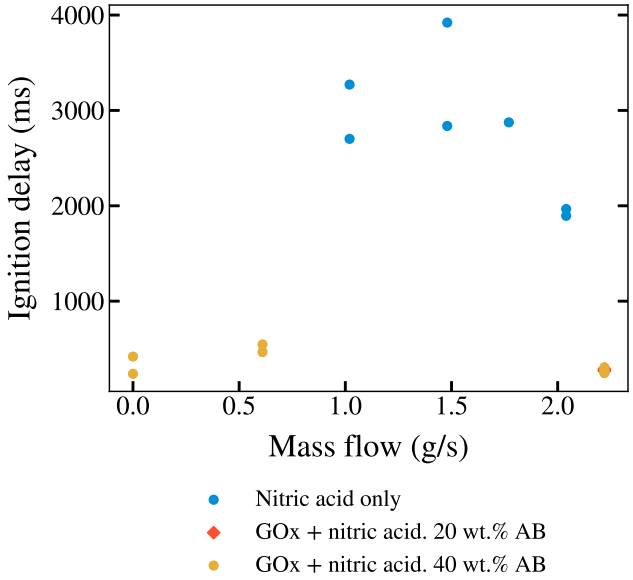

Fig. 19. Comparison of the ignition delay as a function of the oxidizer mass flow. In the cases when only nitric acid is used, the mass flow corresponds to the nitric acid mass flow from the injector. In the case when GOx is also used, the mass flow corresponds to the GOx flow rate.

for 1.02 g/s, 1.48 g/s and 1.77 g/s, respectively. However, at 2.04 g/s the ignition delay decreases by approximately 1 s (30%) to reach 1931 ms. The exact mechanism for this decrease in ignition delay is not known, but many hypotheses are proposed. First, the higher injection pressure increases oxidizer droplet velocity and flow rate. The increased droplet velocity has previously been shown to reduce the ignition delay of hypergolic hybrid fuels due to the increased surface coverage upon splashing of the droplets [4,6,16]. This increased surface contact between the nitric acid and AB increases the likelihood of meeting the conditions for hypergolic ignition. In addition to the increased surface area covered by the acid, the increased droplet momentum changes the dynamics of the agglomerated oxidizer pool. The pool appears to creep along the surface of the fuel, leaving a thin layer of oxidizer in its wake. The large variation in oxidizer thickness and amount on the fuel surface may also increase the likelihood of reaching hypergolic ignition conditions. Finally, it is also possible that under the first three pressure conditions, there is not enough oxidizer to achieve ignition quickly. However, if this explanation was the key factor in explaining the difference in ignition delay, there should have been a decrease in ignition delay between the 1.04 g/s tests and the 1.77 g/s tests, which is not the case here.

3.5. Reignition

One of the most important aspects of a hypergolic hybrid engine often discussed but rarely tested, either in droplet ignition tests or in engine conditions, is its reignition capability. In theory, a hypergolic hybrid engine could be shut down and reignited by simply closing and reopening the oxidizer flow into the combustion chamber. However, as several research studies show, during hypergolic ignition drop tests, ammonia borane and paraffin samples tend to form a black foam-like deposit on their surface, which can potentially reduce hypergolic performance during subsequent relights.

In the experiments conducted here, several reignition tests were performed. Among the tests performed when nitric acid is the sole oxidizer, 5 out of 6 tests successfully reignited. However, the ignition delay for each reignition is much longer than the initial hypergolic ignition. The reignition delays are 6681, 4000, 3820, 2573 and 8379 ms for tests with mass flow rates of 1.04 g/s, 1.04 g/s, 1.48 g/s, 2.04 g/s and 2.04 g/s, respectively. The longer ignition delay can be explained by the completely different fuel surfaces between virgin and previously burned sample. After the initial hypergolic burn, the surface is irregular, with large peaks and valleys of melted paraffin that solidified between the two burns. Char and condensed combustion products are also observed sitting on the surface. In some cases, burn-through of the sample at the site of initial ignition is visible. The altered exposed surface is unlikely to maintain the same additive content as the initial burn, thus affecting the ignition delay. However, the altered conditions remain similar to what the surface would be under real engine conditions. Thus, the ignition delay of the hypergolic reignition sample is something worth looking at in extended studies focused on this particular problem. This does not change the fact that the results are considered significant because they demonstrate the successful reignitability behavior of paraffin/AB hypergolic fuels with sprayed nitric acid as the oxidizer. In addition, reignition experiments were also performed on 3 tests when GOx is the main oxidizer following ignition. The measured IDs are 2492, 1796, and 278 ms, with the first two tests containing 40 wt% AB and the last containing 20 wt% AB. The IDs are again lower than those when GOx is not used, but are still significantly higher than for the first hypergolic ignition in the same conditions. These results indicate that GOx contributes to the reduction of the ignition delay even in the case of reignition. However, its addition to the reactants is not sufficient to overcome the fact that the exposed fuel surface seems to be the limiting factor inhibiting fast reignitions.

4. Discussion

4.1. Mechanisms of hypergolic ignition and comparison with droplet and spray ignition tests

It is believed that paraffin does not react with the oxidizer until it begins to evaporate after hypergolic ignition. Its primary role prior to ignition is to act as a binder for AB, but it also acts as a sink for the heat generated by the exothermic reactions between AB and nitric acid. The initiation reaction between AB and nitric acid is likely to produce oxides and hydrogen gas through a highly exothermic process [25]. The heat generated by this reaction leads to a temperature rise, which facilitates a self-reaction of the nitric acid, likely producing the oxidant dinitrogen pentoxide (N_2O_5) and water [26].

Upon contact between nitric acid and AB, the orange gas observed indicates that the oxidant is decomposing into N_xO_y oxides. For example, N_2O_3 is formed by the decomposition of N_2O_5 [26], or NO and NO_2

are formed by the self-reaction of HONO and nitric acid [27,28]. This observation is also consistent with the results of Baier et al. [29], who attributed this gas to the formation of NO_2. At this point, the conditions for successful ignition are present, namely the gaseous presence of strong oxidants and fuels, as well as a high temperature. Baier et al. [29] experimentally observed the exothermic formation of HBO_2 prior to ignition, suggesting that it also contributes to the heat release that drives the decomposition of nitric acid.

Once ignited, the flame transfers its heat to the solid fuel sample, contributing to both the vaporization of paraffin and the decomposition of AB. The latter is known to produce H_2 and other secondary species (H_2BNH_2, B_2H_6, NH_3, and $B_3H_6N_3$) [25].

Experiments using oxygen and nitric acid for hypergolic ignition show significantly shorter ignition delays compared to when only nitric acid is used. Filling the combustion chamber with oxygen before injecting nitric acid reduced the ignition delay tenfold, from up to 3 s to about 280 ms. The major difference is that an oxidizing species (O_2) is already available as a gas to react with the species formed by the decomposition of nitric acid, thus limiting the steps required to achieve ignition and bypassing the thermal decomposition step of nitric acid when used as the sole oxidizer.

Nevertheless, the ignition delays measured using nitric acid as the sole oxidizer are surprisingly higher than the spray ignition tests (between 300 to 1100 ms, [6]) and droplet ignition tests of previous studies (between 20 to 45 ms, [5]). The difference in ignition delay compared to droplet tests is at least partly due to the slower oxidizer supply to the fuel for spray delivery, resulting in a longer time to reach optimal local O/F ratio for ignition. In spray delivery, the oxidizer is delivered gradually, which does not allow the local O/F ratio to reach its optimal value as quickly. Moreover, the combustible gases emitted by the hypergolic additives at the surface can be cooled down or blown away by the gaseous flow entrained by the oxidizer spray. Too much oxidizer will quench the flame, while too little will not result in enough generated heat for combustion. The confinement in the slab burner probably enhances this entrainment effect for outgassing, as opposed to spray ignition tests conducted in an open environment. Moreover, there is a stochastic aspect to hypergolic ignition, as discrete additive particles need to come into contact with the oxidizer to ignite. This is less likely to happen when the oxidizer is delivered as a spray, as opposed to a large droplet covering the entire fuel surface at once. All these factors contribute to the longer ignition delays observed in the current study.

It is worth noting that as described by Pfeil [30], an ignition delay longer than 10 ms may subject an engine to a hard-start during ignition. This makes the ignition of engines using high flow oxidizer spray injectors susceptible to failure during ignition. It is worth noting that in a droplet ignition test configuration, the current combination of additive, paraffin and nitric acid can ignite under 10 ms, as presented in our previous experiments [5]. As it is the case with our previous spray ignition experiments [6], the results presented here suggest that a low-flow oxidizer spray is also capable of leading to successful ignition and flame propagation within a combustion chamber.

Additionally, another difference explaining the ignition delay measured previously in spray ignition tests (from 300 to 1100 ms [6]) and here (2000 to 4000 ms) may be due to the fact that the combustion chamber is filled with nitrogen as opposed to ambient air, which limits the amount of O_2 available in the environment to initiate the ignition. In addition, the fact that the injector is placed in the same direction as the fuel, as opposed to having its tip pointing directly at the sample as in the spray ignition tests, may reduce the splashing of the droplet hitting the surface. This would limit the surface area covered by nitric acid and delay the hypergolic ignition. The results presented here indicate that, in addition to the introduction of nitric acid into the combustion chamber, the introduction of gaseous oxidants such as GOx may be a suitable alternative to reduce the ignition delay of hypergolic hybrid engines.

4.2. Regression rate

Finally, the regression rate of the fuel was examined. Unfortunately, image analysis algorithms, such as those presented by Jobin et al. [19] or Dunn et al. [31], could not be implemented here to determine the regression rate due to the accumulation of oxidizer and melted paraffin on the windows. Even if the use of such an algorithm would have been possible, it is uncertain whether the results would have been of much value due to the fact that the fuel samples tend to swell during combustion, thus initially presenting a negative regression rate. This observation was also made by Pfeil in the combustion of a small WFNA-paraffin/AB hybrid engine [30].

In an effort to estimate this interesting metric, the regression rate is obtained by measuring the difference in mass before and after each test. The following equation is used to convert the mass to a regression rate value:

$$\dot{r} = \frac{\Delta m}{\rho_{fuel} \cdot A \cdot t_b} \tag{10}$$

where $\dot{r}$ is the regression rate, Δm is the mass difference, ρ_{fuel} is the density of the fuel mixture, with 900 kg/m^3 as the density of paraffin and 780 kg/m^3 as the density of AB, $A = 114.3\ x\ 50.8$ mm^2 is the area exposed to the fuel, and t_b is the burn time. However, as noted above, because water is injected into the chamber after each test to dilute the remaining nitric acid, the estimated regression rate values may be higher than reality due to the reaction of AB with the fluid. In addition, this method relies on the ability of the test operators to retrieve each piece of fuel remaining in the combustion chamber. This has proven to be more difficult than anticipated due to the high degradation of fuel samples and their brittleness after combustion. The results are presented in Table 3. While the regression rate values may not be exact, the trends observed follow the expected behavior. First, when GOx and nitric acid are used, the consumed mass per second and the regression rate of the sample are higher when the fuel composition is 40 wt% AB as opposed to 20 wt% for a given injection pressure. This is expected due to the rapid hypergolic reactivity of AB and nitric acid. This observation is also consistent with the results of Benhidjeb-Carayon et al. [17], where they used a higher concentration of hypergolic additives in sections of the fuel in a 2-in hypergolic hybrid engine. The sections of the fuel grain containing the highest amount of additives were completely burned out after their tests, while fuel remained where a lower concentration of hypergolic additives was used. Second, as the GOx flow rate is increased, while keeping the nitric acid flow rate constant, the measured regression rate also increases as shown on Fig. 20. This observation is consistent with the formulation commonly used for hybrid rocket fuels ($\dot{r} = aG_{ox}^n$, where G_{ox} is the oxidizer mass flux).

Finally, for the tests conducted when nitric acid is the only oxidizer, the regression rate increases as the mass flow rate also increases. In both cases, the variability for the $\dot{r}$ values is impossible to quantify, due to the fact that only two tests were conducted. These results should therefore be interpreted with great caution and the completion of the data set will be the subject of future studies.

5. Conclusions

A novel hypergolic slab burner was developed to study the hypergolic ignition of hybrid rocket fuels in an engine-like configuration. The design of the slab burner and its injection system were presented. The spray from the injector was characterized using a Phase Doppler Anemometer system. Two sets of experiments were performed. In the first, paraffin-based fuels containing 20 or 40 wt% of ammonia borane were used. The gaseous oxidizer was first introduced into the combustion chamber and 90% concentrated nitric acid was then injected for a few seconds to initiate combustion. In the second set of experiments, the combustion chamber was filled with nitrogen, then nitric acid was injected for the entire duration of the test. Both configurations

Table 3
Mass burned and regression rate of each tested configuration. 40–60 refers as 40 wt% AB–60 wt% paraffin fuel mixture and 20-80 refers as 20 wt% AB–80 wt% paraffin fuel mixture.

Oxidizer	Nitric acid flow rate [g/s]	GOx flow rate [g/s]	Fuel	Δm [g/s]	$\dot{r}$ [mm/s]
Nitric acid + GOx	1.48	2.22	20–80	0.36 ± 0.05	0.07 ± 0.01
	1.48	0	40–60	0.13 ± 0.04	0.03 ± 0.01
	1.48	0.61	40–60	0.22 ± 0.00	0.04 ± 0.00
	1.48	0.88	40–60	0.41 ± 0.06	0.08 ± 0.01
	1.48	2.22	40–60	0.35 ± 0.10	0.07 ± 0.02
Nitric acid	1.02	N/A	40–60	0.38 ± 0.16	0.08 ± 0.03
	1.48	N/A	40–60	0.57 ± 0.08	0.12 ± 0.02
	2.04	N/A	40–60	0.75 ± N/A	0.15 ± N/A

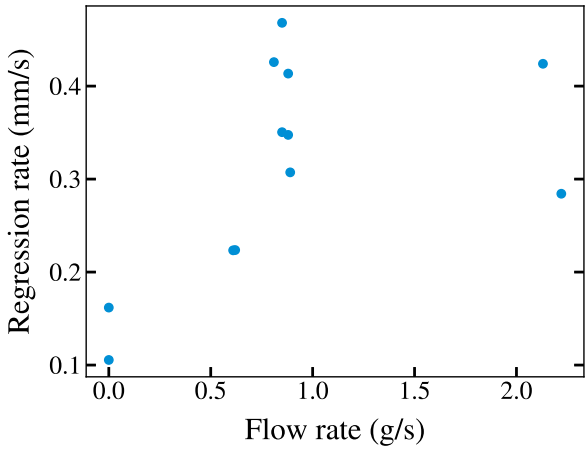

Fig. 20. Regression rate as a function of GOx mass flow rate at a constant nitric acid flow rate of 1.48 g/s for fuel samples containing 40 wt% AB.

successfully led to hypergolic ignition that transitioned to sustained combustion. The ignition delay of the first set of experiments was more than 10 times lower than that of the second set. Finally, the reignition of these fuels was investigated. All reignition tests conducted with the first experimental configuration successfully reignited, while the success rate in the second configuration was 83%. In both configurations, the ignition delay is greater than when the sample was first ignited. This is attributed to the change in the exposed surface of the fuel, namely char deposition, melted paraffin coating the surface, and uneven additive content. This novel test apparatus paves the way for the study and understanding of the phenomena behind hypergolic ignition. Further testing with new instrumentation and other fuel/oxidizer combinations will be the focus of future studies. In addition, a method for spatially and temporally measuring the regression rate should be implemented to take full advantage of the slab burner.

CRediT authorship contribution statement

Olivier Jobin: Writing – original draft, Software, Methodology, Investigation, Conceptualization. **Mathieu Chartray-Pronovost:** Writing – review & editing, Investigation. **William Kaprolat:** Writing – review & editing, Investigation. **Étienne Robert:** Writing – review & editing, Conceptualization.

Declaration of competing interest

The authors declare that they have no known competing financial interests or personal relationships that could have appeared to influence the work reported in this paper.

Acknowledgments

This work was supported by the Natural Sciences and Engineering Research Council of Canada (NSERC) RGPIN-2022-05071; NSERC CGS M (to O.J.), and ES D scholarships (to O.J. and M.C.-P.) and the Canadian Space Agency Flights and Fieldwork for the Advancement of Science and Technology (FAST) funding initiative grant 18FAPOLB17.

Appendix A. Supplementary data

Supplementary material related to this article can be found online at https://doi.org/10.1016/j.combustflame.2024.113948. Videos of some tests are available online as supplemental content. Additional data is available upon request.

References

[1] M. Pfeil, A.S. Kulkarni, P.V. Ramachandran, S.F. Son, S.D. Heister, Solid Amine–Boranes as high-performance and hypergolic hybrid rocket fuels, J. Propul. Power 32 (2016) 23–31.
[2] M.J. Baier, P.V. Ramachandran, S.F. Son, Characterization of the hypergolic ignition delay of ammonia borane, J. Propul. Power 35 (2018) 182–189.
[3] V.K. Bhosale, J. Jeong, S. Kwon, Ignition of boron-based green hypergolic fuels with hydrogen peroxide, Fuel 255 (2019) 115729.
[4] K.A. Clements, M.J. Baier, P.V. Ramachandran, S.F. Son, Experimental study of factors affecting hypergolic ignition of ammonia borane, J. Propul. Power 37 (2021) 202–210.
[5] B. Elzein, O. Jobin, E. Robert, Reducing the ignition delay of hypergolic hybrid rocket fuels, J. Propul. Power 37 (2021) 77–85.
[6] O. Jobin, B. t Dumas, J. Zahlawi, M. Chartray-Pronovost, É. Robert, Hypergolic ignition of paraffin-based hybrid rocket fuels by sprays of liquid oxidizer, Proc. Combust. Inst. 39 (2023) 5073–5082.
[7] B. Dumas, O. Jobin, W. Kaprolat, J. Zahlawi, E. Robert, Ignition delay and performance of sorbitol based hypergolic hybrid fuels, Fuel 349 (2023) 128417.
[8] O. Jobin, C. Mottillo, H.M. Titi, J.M. Marrett, M. Arhangelskis, R.D. Rogers, B. Elzein, T. Friščić, É. Robert, Metal–organic frameworks as hypergolic additives for hybrid rockets, Chem. Sci. 13 (2022) 3424–3436.
[9] H.M. Titi, J.M. Marrett, G. Dayaker, M. Arhangelskis, C. Mottillo, A.J. Morris, G.P. Rachiero, T. Friščić, R.D. Rogers, Hypergolic zeolitic imidazolate frameworks (ZIFs) as next-generation solid fuels: Unlocking the latent energetic behavior of ZIFs, Sci. Adv. 5 (2019) 1–8.
[10] K. Wang, Z. Wang, X. Zhao, X. Qi, S. Song, Y. Jin, Q. Zhang, Unearthing hidden hypergolic potential of energetic complexes with hydrogen peroxide, Combust. Flame 244 (2022) 112235.
[11] A. Benhidjeb-Carayon, M.P. Drolet, J.R. Gabl, T.L. Pourpoint, Reactivity and hypergolicity of solid fuels with mixed oxides of nitrogen, J. Propul. Power 35 (2019) 466–474.
[12] D.A. Castaneda, B. Natan, Experimental investigation of the hydrogen peroxide – solid hydrocarbon hypergolic ignition, Acta Astronaut. 158 (2019) 286–295.
[13] S. Nath, I. Laso, J. Lefkowitz, Parametric ignition study of a green hypergolic hybrid rocket fuel, in: AIAA SCITECH 2022 Forum, Paper 2022-1484, 2022.
[14] S. Nath, I. Laso, L. Mallick, Z. Sobe, S. Koffler, B. Blumer-Ganon, E. Borzin, N. Libis, J.K. Lefkowitz, Comprehensive ignition characterization of a non-toxic hypergolic hybrid rocket propellant, Proc. Combust. Inst. 39 (2023) 3361–3370.
[15] B. Dumas, O. Jobin, É. Robert, Multiple diagnostics of hybrid rocket ignition and effect of hypergolic additive granulometry, J. Propul. Power 40 (2024) 497–506.
[16] S. Nath, L. Mallick, J. Lefkowitz, Spray ignition studies on a green hypergolic hybrid rocket propellant, in: AIAA SCITECH 2023 Forum, Paper 2023-1831, 2023.

[17] A. Benhidjeb-Carayon, J.R. Gabl, B.E. Whitehead, T.L. Pourpoint, Hypergolic hybrid rocket engine ignition and relights with mixed oxides of nitrogen, J. Propul. Power 38 (2022) 111–121.
[18] J. Jeong, K.-S. Kim, V.K. Bhosale, S. Kwon, Demonstration of ammonia borane-based hypergolic ignitor for hybrid rocket, Acta Astronaut. 196 (2022) 85–93.
[19] O. Jobin, Small-Scale Experiments for the Development and Characterization of Novel Hypergolic Hybrid Rocket Fuel Systems (Ph.D. thesis), Polytechnique Montreal, 2023.
[20] E.T. Jens, A.C. Karp, V.A. Miller, G.S. Hubbard, B.J. Cantwell, Experimental visualization of hybrid combustion: Results at elevated pressures, J. Propul. Power 36 (2019) 33–46.
[21] C. Glaser, R. Gelain, A. Bertoldi, Q. Levard, J. Hijlkema, J.-Y. Lestrade, P. Hendrick, J. Anthoine, Experimental regression rate profiles of stepped fuel grains in hybrid rocket engines, Acta Astronaut. 204 (2023) 186–198.
[22] A.H. Lefebvre, V.G. Mcdonell, Atomization and Sprays, Taylor & Francis Group, U.S., 2017.
[23] C. Indiana, M. Bellenoue, B. Boust, Experimental investigations of drop size distributions with impinging liquid jets using phase doppler anemometer, Int. J. Energetic Mater. Chem. Propul. 14 (2015) 241–264.
[24] C. Glaser, J. Hijlkema, J. Anthoine, Evaluation of regression rate enhancing concepts and techniques for hybrid rocket engines, Aerotec. Missili Spaz. 101 (2022) 267–292.
[25] M.R. Weismiller, A.C.T. van Duin, J. Lee, R.A. Yetter, ReaxFF reactive force field development and applications for molecular dynamics simulations of ammonia borane dehydrogenation and combustion, J. Phys. Chem. A 114 (2010) 5485–5492.
[26] D.J. Ladanyi, R.O. Miller, W. Karo, C.E. Feiler, Some fundamental aspects of nitric acid oxidants for rocket applications, Nasa Technical Report #NACA-RM-E52J01, 1953.
[27] E.W. Kaiser, C.H. Wu, Measurement of the rate constant of the reaction of nitrous acid with nitric acid, J. Phys. Chem. 81 (3) (1977) 187–190.
[28] W.H. Chan, R.J. Nordstrom, J.G. Calvert, J.H. Shaw, Kinetic study of nitrous acid formation and decay reactions in gaseous mixtures of nitrous acid, nitrogen oxide (NO), nitrogen oxide (NO2), water, and nitrogen, Environ. Sci. Technol. 10 (7) (1976) 674–682.
[29] M.J. Baier, A.J. McDonald, K.A. Clements, C.S. Goldenstein, S.F. Son, High-speed multi-spectral imaging of the hypergolic ignition of ammonia borane, Proc. Combust. Inst. 38 (2021) 4433–4440.
[30] M. Pfeil, Solid amine-boranes as high performance hypergolic hybrid rocket fuels (Ph.D. thesis), Purdue University, 2014.
[31] C. Dunn, G. Gustafson, J. Edwards, T. Dunbrack, C. Johansen, Spatially and temporally resolved regression rate measurements for the combustion of paraffin wax for hybrid rocket motor applications, Aerosp. Sci. Technol. 72 (2018) 371–379.